Smart Power Management of DC Microgrids in Future Milligrids

Peyghami, Saeed; Mokhtari, Hossein; Davari, Pooya; Loh, Poh Chiang; Blaabjerg, Frede

Published in:
Proceedings of 18th European Conference on Power Electronics and Applications (EPE'16 ECCE Europe), 2016

DOI (link to publication from Publisher):
10.1109/EPE.2016.7695459

Publication date:
2016

Document Version
Accepted author manuscript, peer reviewed version

Smart Power Management of DC Microgrids in Future Milligrids

Saeed Peyghami-Akhuleh, Hossein Mokhtari
Sharif University of Technology
Tehran, Iran
Tel: +98 (21) 66165974
Fax: +98 (21) 66023261
saeed_peyghami@ee.sharif.edu,
mokhtari@sharif.edu
http://www.ee.sharif.edu

Pooya Davari, Poh Chiang Loh, Frede Blaabjerg
Aalborg University
Alborg, Denmark
Tel: +45 9940 9254
Fax: +45 9815 1411
pda@et.aau.dk, pcl@et.aau.dk,
fbl@et.aau.dk
http://www.et.aau.dk

Keywords

«Microgrid», «Smart grids», «Smart microgrids», « Power management».

Abstract

In this paper a novel droop approach for power management in low voltage dc MicroGrids (MGs) based on a master-slave concept is presented. A virtual frequency is injected by a master unit, which is proportional to its output power. Other slave units determine their output power according to the corresponding frequency based droop characteristics. Unlike the dc voltage-droop methods, the proposed virtual frequency-droop approach can be smartly applied for proportional power management among the energy units and loads as well as adding zero net energy capability to the MG. Both power flow and energy flow can be performed without utilizing an extra communication system. Simulation results validate the effectiveness of the proposed scheme.

I. INTRODUCTION

The concept of ac/dc MGs has been proposed in recent years to increase reliability, power quality and decrease losses and pollution. Future distribution systems will consist of many interconnected ac and dc MGs to form the milligrids. Hence these MGs will be the dynamically decoupled cells of the milligrids [1]. Integrating Renewable Energy Resources (RERs) and storages into the distribution systems to enhance the overall reliability and efficiency, requires proper power sharing control algorithms by employing the MG and smart grid technologies [2]–[4]. Furthermore, dc MGs are more applicable, reliable and efficient systems to integrate many power sources and loads, such as PhotoVoltaic (PV) modules, Fuel Cell (FC) units, batteries, motor driven loads, and full converter based generators (i.e. micro-turbines and wind turbines), which naturally have a dc coupling.

In respect to the potential use of RERs and Distributed Storages (DSs) in the vicinity of the loads in MGs, they can be dispatched as zero-net-energy units which create the opportunity to reduce the overall impact of energy generation and transmission on economy, climate, and ecology [5]. Zero or low energy exchange between the grid and MG during a period can be obtained by proper sizing of Energy Units (EUs). On the other hand, DSs such as battery banks in MGs, play an important role on adjusting the variable power of RERs with load profile as well as improving the reliability by supporting the MG in the islanded mode [4], [6]. Therefore, DSs can be employed to form a dynamically decoupled MG by regulating the dc voltage and managing power and energy in the MG at grid connected and islanded mode.

To have a stable operation in a dc MG, appropriate load sharing controller, and voltage regulator are required. Some droop approaches based on dc voltage at primary level have been applied to dc MGs to properly control the load sharing and improve the stability of the MG. However, voltage based droop methods suffer from poor voltage regulation and load sharing [7]–[12], since the voltage is a local

variable, and hence, the voltage has not the same value all over the grid to coordinate different EUs and loads. Considering line resistances in the case of long feeders, the performance of the droop methods is not satisfactory. To increase the accuracy of the load sharing, large droop gains should be employed at primary level. Larger droop gains cause higher voltage drop in the case of dynamically stable operation condition. To overcome these issues, average current sharing approaches reinforced by communication infrastructures have been presented in [13]–[15], which affects the overall system reliability and stability [11].

To overcome these issues, a novel smart power sharing control system based on a master-slave concept is proposed in this paper. A DS is considered as a master unit to inject a small ac voltage with a virtual frequency (f_v) related to its output current. Other units locally extract this frequency to control the output currents according to the proposed droop characteristics. Since the frequency has the same value all over the MG, it can be carried out not only to coordinate all type of DGs and DSs but also to curtail the non-critical loads. The main objectives of the proposed control system are:

- *Proportional load sharing among DGs and DSs*
- *Smart power exchange between MG and local grid*
- *Smart energy management and load shedding*
- *Zero/low net energy exchange between MG and local grid*
- *Operating in both grid connected and islanded modes without changing control algorithm*
- *Increasing the reliability because of communication-free control approach*

II. PROPOSED CONTROL APPROACH AND OPERATING MODES

All EUs in MGs can be categorized into Distributed Generators (DGs), DSs and local ac or dc grid as summarized in TABLE I. In the proposed control scheme, only a battery bank (i.e., DS) is selected as a master unit. It has a fast response to the load variation, and is also employing suitable Energy Management System (EMS) makes it available to support the MG at different loading and sourcing conditions. Other types of EUs are considered to operate as slave units according to the proposed droop characteristics. However, non-dispatchable units normally operate at Maximum Power Point Tracking (MPPT) mode. Once the generated power exceeds the load, the control system of these types of DGs seamlessly will be switched to non-MPPT mode.

To explain the control strategy, a simplified dc MG with different type of EUs is considered as shown in Fig. 1, where the battery is the master, and the slave units include an FC as a dispatchable DG, a PV as a non-dispatchable DG, and an Interlinking Converter (IC) as a local grid converter. Both ac and dc grids are feasible as a local grid in the future distribution systems. Here a dc grid is considered. Furthermore, non-critical loads are contemplated for load shedding at heavy load conditions. In general, the non-dispatchable units can be controlled like the PV, the dispatchable DGs and DSs can be operated like the FC as considered in Fig. 1.

Table I: Classification of Different Distributed Sources and Storages

Source Type	Specification	Example	Master/Salve
Distributed Generators	Dispatchable	Fuel Cell, Micro-Turbine	Slave
	Non-dispatchable	Photovoltaic, Wind Turbine	MPPT/Slave
Distributed Storages	Dispatchable/Fast	Battery	Master
	Dispatchable/Slow	Fly Wheel, Regenerative Fuel Cell	Slave
Local Grid	Dispatchable (in grid connected mode)	Local DC or AC Grid	Slave

A. Control Approach

A flow chart of the proposed control system is shown in Fig. 2. As it can be seen in Fig. 2 (a), the battery unit as a master, measures the output current and injects a small ac voltage with a frequency, called virtual frequency (f_v), into the MG. The relation between the virtual frequency (f_v) and the battery current (I_b) can be determined as (1). This relation is shown in Fig. 3 (a).

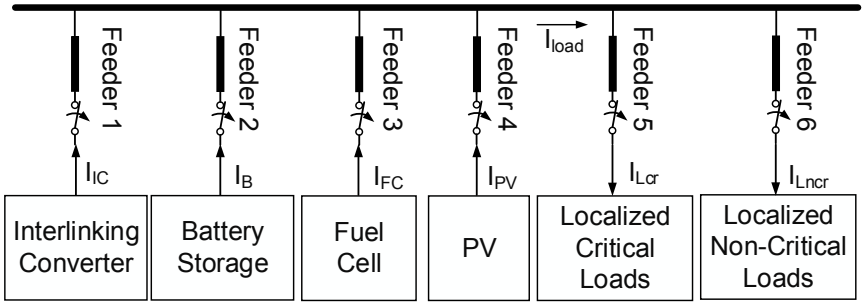

Fig. 1. Simplified dc MG with Battery as a master, Fuel Cell as a dispatchable DG, PV as a MPPT based slave, Local Grid Interlinking Converter as a slave unit, and localized critical and non-critical loads.

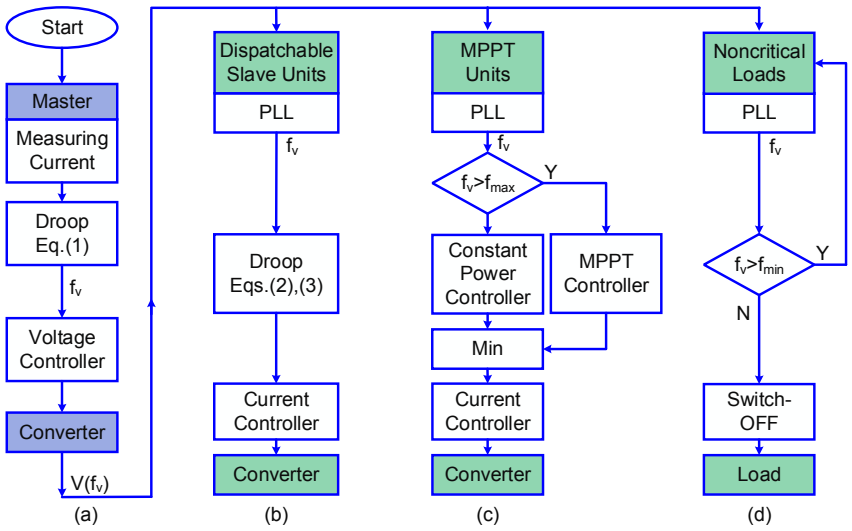

Fig. 2. Flow chart of control algorithm for (a) master unit, (b) dispatchabe units, (c) non-dispatchable units, and (d) non-critical loads.

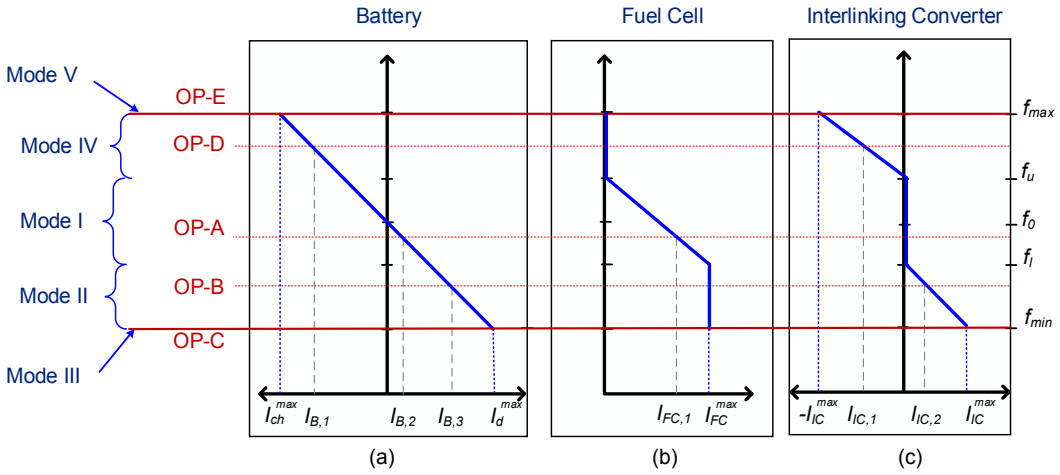

Fig. 3. Proposed droop control scheme: (a) droop characteristic of battery, (b) droop characteristics of Fuel Cell, and (c) droop characteristic of Interlinking Converter.

$$f_v = f_0 - \frac{f_{\max} - f_{\min}}{I_d^{\max} + I_{ch}^{\max}} I_B \tag{1}$$

where f_{max} and f_{min} are the maximum and minimum frequencies, $I_{ch}^{\max}$ and $I_d^{\max}$ are the maximum charging and discharging currents of the battery. The energy level of the battery needs to be controlled to ensure proper supporting of the MG. Hence, the proposed droop equation of the battery should be tuned based on the State Of Charge (SOC) level of the battery. This procedure is explained in the subsection C.

As shown in Fig. 2 (b), the dispatchable units such as FC and IC, locally measure the f_v and controls the output current based on a desired droop characteristics. Here, the droop characteristics for the FC and IC are defined as (2) and (3), respectively.

$$I_{FC} = \begin{cases} 0 & f_u \le f_v \\ \dfrac{I_{FC}^{\max}}{f_l - f_u}(f_v - f_u) & f_l \le f_v \le f_u \\ I_{FC}^{\max} & f_v \le f_l \end{cases} \tag{2}$$

$$I_{IC} = \begin{cases} -\dfrac{I_{IC}^{\max}}{f_{\max} - f_u}(f_v - f_u) & f_u \le f_v \\ 0 & f_l \le f_v \le f_u \\ \dfrac{I_{IC}^{\max}}{f_{\min} - f_l}(f_v - f_l) & f_v \le f_l \end{cases} \tag{3}$$

where $I_{FC}^{\max}$ is the rated current of FC and the upper and lower frequencies are denoted as f_u and f_l, which determine the operating interval of the FC. The droop characteristics of the FC is shown in Fig. 3 (b).

The IC operates based on the droop equation in (3), which is shown in Fig. 3 (c), where $I_{IC}^{\max}$ is the rated power. Once the frequency stays between f_u and f_l , the output power of the IC is settled at zero. However, when the load exceeds the power of the local EUs, the frequency drops under f_l, and the load should be supplied by the IC. Moreover, when the generated power of the local units exceeds the required demand of the MG, the output power of the FC should be zero and the excess power of the PV needs to be absorbed by the IC and battery. In this case, the frequency rises more than f_u. Notably, the proposed droop characteristics for the IC results in zero/low net energy exchanging between the MG and local grid during a period. Furthermore, disconnection of the IC does not affect the operation of the MG since it is controlled as a slave unit.

Non-dispatchable units normally operate at MPPT mode, whenever the power exceeds the load, battery, and IC power, frequency reaches the maximum value f_{max}. As it can be seen in Fig. 2 (c), the PV control unit measures the f_v and when it reaches the maximum value it forces the PV to operate at non-MPPT mode [16], [17].

As shown in Fig. 2 (d), non-critical loads can be turned off by locally measuring the frequency. This is due to the fact that load shedding must be applied at some points in the case of lower generation and storage in the MG. If the frequency is lower than the minimum frequency, the load will be turned off.

To ensure a reliable operation of the system, redundant battery units (i.e., master units) is a must to consider.

B. Operating Modes

Based on the virtual frequency which is related to the demand of MG, five different operating modes can be considered as shown in Fig. 3.

1) **Mode I:** in this mode, loads are demanded by the local EUs (FC, PV and battery) and the exchanged power with the grid is zero. The virtual frequency f_v is between f_u and f_l. As it can be seen in Fig. 3, the Operating Point A (OP-A) the output current of the IC is zero, the output current of FC and battery are $I_{FC,1}$ and $I_{B,2}$, respectively. Hence, the load current I_{load} can be determined as:

$$I_{load} = I_{FC,1} + I_{B,2} + I_{PV} \tag{4}$$

where I_{pv} is the PV current and PV works at the MPPT mode.

2) **Mode II:** in this mode, the loads are exceeded to the rated power of the FC and output current of the PV, thus, the frequency drops down and the MG needs to be supported by the grid. Considering the OP-B the load current can be calculated as:

$$I_{load} = I_{IC,2} + I_{FC}^{\max} + I_{B,3} + I_{PV} \tag{5}$$

where $I_{IC,2}$ and $I_{B,3}$ are the current of IC and battery respectively.

3) **Mode III:** if the load exceeds the rated current of all units, the load shedding should be applied to non-critical loads. They can smartly be disconnected from the grid by measuring the frequency. The maximum load supplied by the units at OP-C is:

$$I_{load} = I_{IC}^{\max} + I_{FC}^{\max} + I_{d}^{\max} + I_{PV} \tag{6}$$

4) **Mode IV:** whenever, the output current of the PV exceeds the local load, it can be injected to the grid and the battery. Hence, in this condition the virtual frequency f_v is between f_u and f_{max}, the FC is in the off state and the excess current is injected into the grid and the battery. For example at OP-D the load current can be determined by (7), where $I_{IC,1}$ and $I_{B,1}$ are the current of the IC and the battery.

$$I_{load} = -I_{IC,1} - I_{B,1} + I_{PV} \tag{7}$$

5) **Mode V:** if the output current of the PV exceeds the maximum currents of the IC, battery and load, its control system needs to be switched to the non-MPPT mode to fix the frequency at $f_v = f_{max}$. Therefore, the output current of the PV at OP-E can be calculated as:

$$I_{PV} = I_{IC}^{\max} + I_{ch}^{\max} + I_{load} \tag{8}$$

C. Battery Droop Tuning

To increase the availability of the battery energy as a master unit to support the MG, a charging and discharging procedure has to be controlled (see Fig. 4). Most batteries have a form of EMS to monitor local quantities like voltages, currents, temperature, humidity, and etc., before concluding on the present SOC, life cycle and other operating details of the batteries. The deduced details can in turn be used to tune the charging and discharging procedures of the storage, which for the characteristics in (1), it can simply be achieved by adjusting $I_d^{\max}$ and $I_{ch}^{\max}$. For instance, if it is required to fully charge the storage before allowing it to discharge, $I_d^{\max}$ can initially be set to zero as in Fig. 4 (a). The discharging process is thus inhibited until its SOC reaches close to 100%. Simultaneously, $I_{ch}^{\max}$ can be dropped to zero in Fig. 4 (b) to prevent charging when the SOC is still high [18].

D. Control of Converters

The structure of the battery converter and IC are considered as a bidirectional boost converter as depicted in Fig. 5 (a). However, as shown in Fig. 5 (b) the FC and the PV are connected using the conventional unidirectional boost converter. The employed parameters of the converters are given in the corresponding figures. Block diagrams of the proposed control algorithms for each unit are illustrated in Fig. 6. Here, Fig. 6 (a) is the control block diagram of the battery as the master unit, Fig. 6 (b) is the control system of the both IC and FC as a dispatchable slave units, and Fig. 6 (c) shows the control system of the PV as a MPPT based unit.

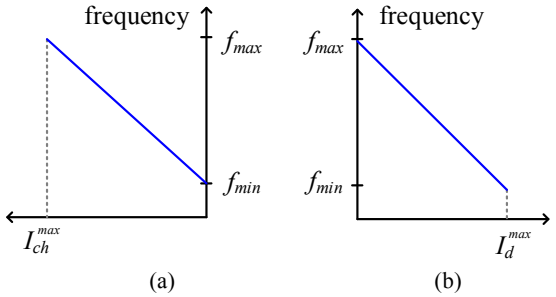

Fig. 4. Battery droop tuning procedure by energy management system, (a) SOC 0%, (b) SOC100%.

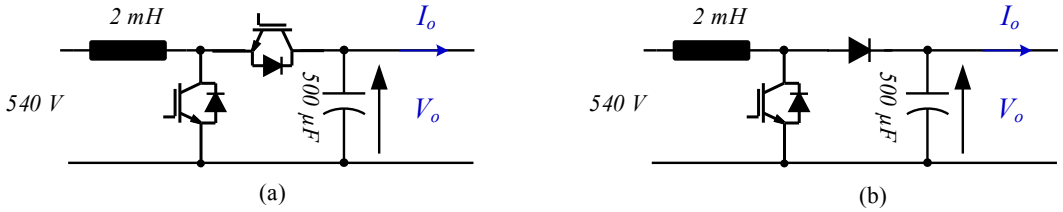

Fig. 5. Converter structure, (a) bidirectional boost converter for battery and IC, (b) unidirectional boost converter for PV and FC.

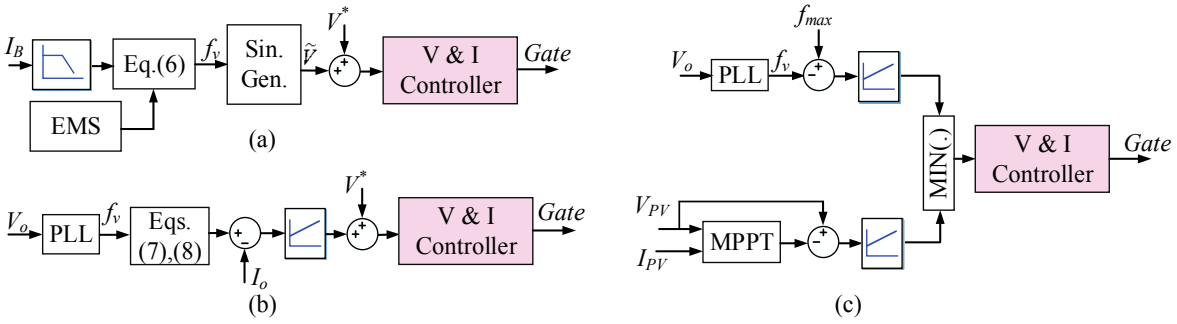

Fig. 6. Block diagram of the control system of (a) battery, (b) slave units (IC and FC), and (c) PV. I_b: output current of battery converter, $\tilde{V}$: small ac voltage, V_o and I_o: output voltage and current of converters, V_{PV} and I_{PV}: input voltage and current of PV.

III. Simulation Results

In order to validate the proposed control approach, a simplified dc MG like the one shown in Fig. 1 is considered. The system parameters are given in TABLE II. Three simulation case studies are presented to validate the performance of the control system in the following.

In Case I, the system is simulated under three different loading conditions and the results are demonstrated in Fig. 7, where Fig. 7 (a) shows the output voltage of EUs with a 5 V peak-peak superimposed ripple, Fig. 7 (b) shows the frequency and Fig. 7 (c) illustrates the output current of DGs. At $0 < t < 2$ *sec*, a no-load condition is considered and consequently the PV operates at MPPT mode. The whole current of the PV is injected into the grid and battery. The FC is off and the frequency is between f_u and f_{max}. Hence following Fig. 3, the system operates at Mode IV. When a 7 *kW* load is connected at $t = 2$ *sec*, the frequency is decreased to 49.8 *Hz* and the operating point is moved to Mode I. Therefore, the IC is switched off and the load will be supplied by the PV, battery and the FC. By increasing the load at $t = 4$ *sec*, the frequency is reduced to 48.96 *Hz* which makes the system to start operating in Mode II. In this mode, the FC operates at rated current and the PV works at MPPT mode, hence, the residual load is properly shared between the IC and battery according to their droop characteristics.

TABLE II: SPECIFICATIONS OF MG AND CONTROL SYSTEM

Definition	Symbol	Value	Definition	Symbol	Value
Rated current of Battery	I_d^{max} - I_{ch}^{max} *(A)*	10	Upper frequency	f_u *(Hz)*	50.5
Rated current of FC	I_{FC}^{max} *(A)*	5	Lower frequency	f_l *(Hz)*	49.5
Rated current of IC	I_{IC}^{max} *(A)*	5	Small AC Voltage	*Peak-Peak (V)*	5
Rated power of PV	P_{MPPT} *(W)*	3750	Feeder 1	$R(\Omega)+jL(\mu H)$	$1+j500$
Nominal dc Voltage	V_{dc} *(V)*	700	Feeder 2	$R(\Omega)+jL(\mu H)$	$0.8+j350$
Rated frequency	f_o *(Hz)*	50	Feeder 3	$R(\Omega)+jL(\mu H)$	$0.7+j300$
Maximum frequency	f_{max} *(Hz)*	51.5	Feeder 4	$R(\Omega)+jL(\mu H)$	$0.6+j250$
Minimum frequency	f_{min} *(Hz)*	48.5	Feeder 5, 6	$R(\Omega)+jL(\mu H)$	$0.5+j350$

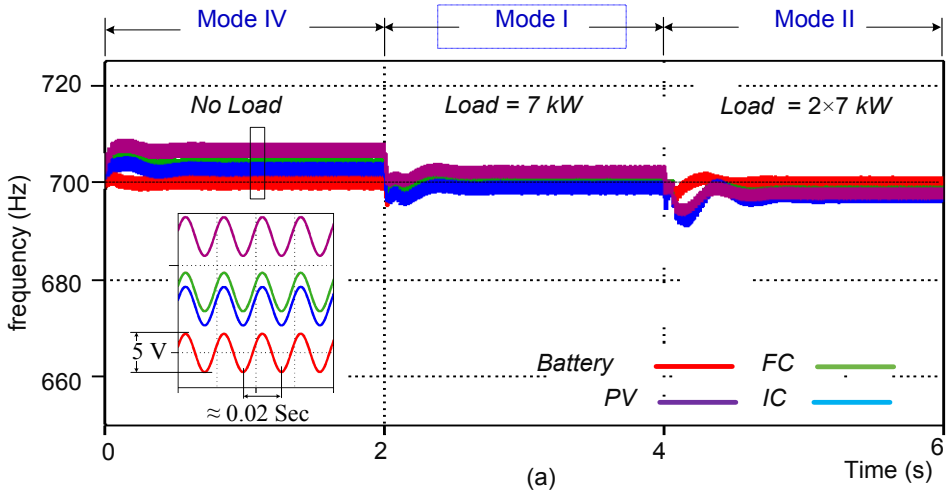

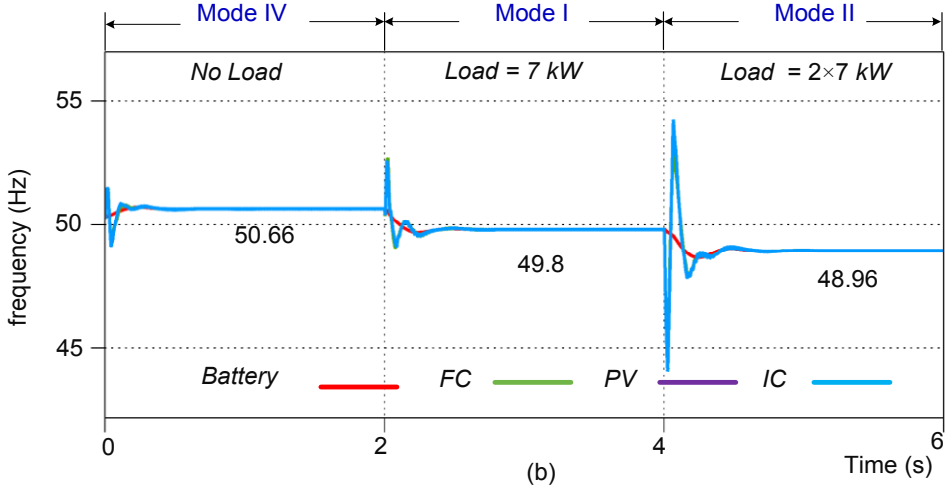

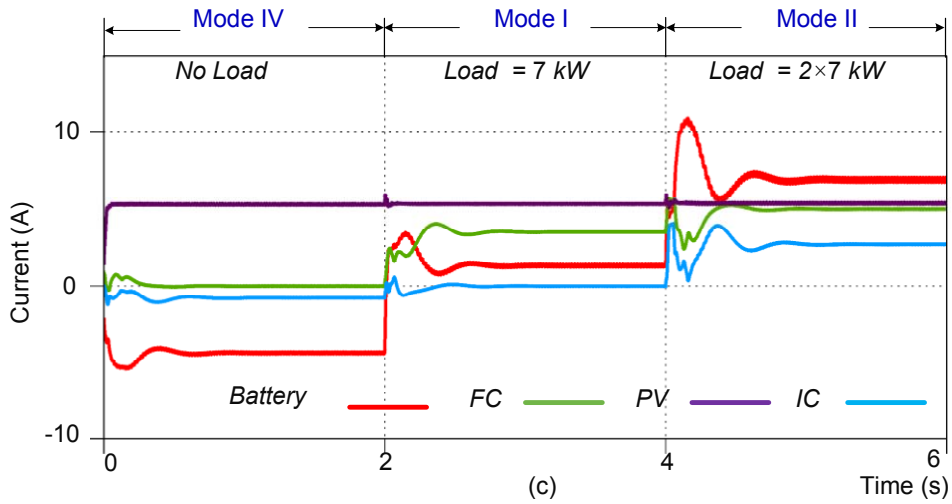

Fig. 7. Simulation Result of Case I: (a) output voltage, (b) frequency, (c) output current of DGs, at $0 < t < 2$ *sec*, the frequency is between the f_u and f_{max} and this operating point is like OP-D. at $2 < t < 4$ *sec*, the frequency is between the f_l and fu like OP-A. at $4 < t < 6$ *sec*, the frequency is between the f_{min} and f_l i.e., OP-B.

In Case II, it is assumed that the SOC of the battery is low, hence the droop characteristics of the battery is adjusted like the one shown in Fig. 4 (a). A 7 *kW* critical load is connected at $t = 2$ *sec*. As shown in Fig. 8, increasing the load causes the frequency drop. Once the frequency drops under the $f_{min} = 48.5$ *Hz*, the local controller switches off a 3.3 *kW* non-critical load at $t = 2.11$ *sec*. Therefore, the frequency is increased and the operating point is moved to Mode II. To prevent unwanted load switching, a low pass filter with 30 *rad/sec* cut-off frequency is considered for non-critical load controller.

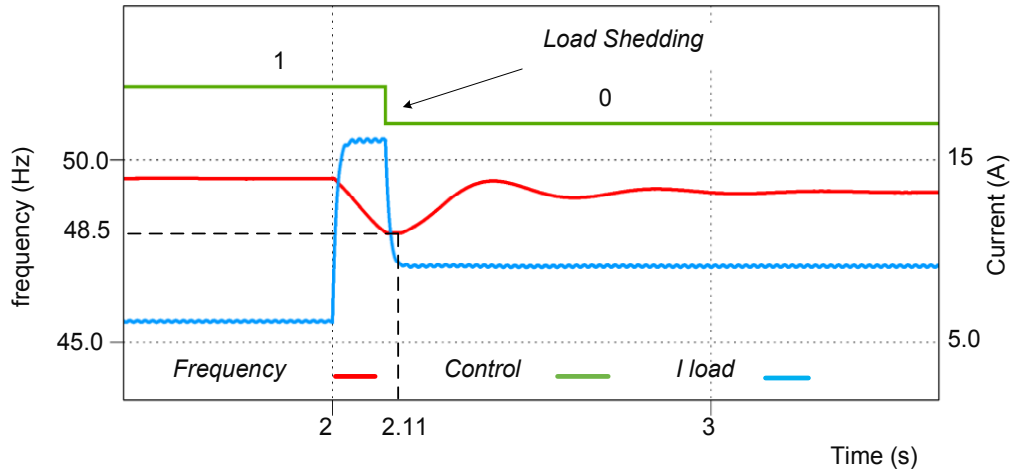

Fig. 8. Simulation results of Case II, critical load is connected at $t = 2$ *sec*, and non-critical load is disconnected at $t = 2.11$ *sec*.

In Case III, it is considered that the battery is fully charged and their droop characteristic is tuned like the one shown in Fig. 4 (b). The IC is also disconnected from the grid and the PV operates at MPPT mode. Two 1.6 *kW* and 4.9 *kW* loads are supported by the battery, PV and the FC. At $t = 2.6$ *sec*, the 4.9 *kW* load is disconnected from the MG. As it can be seen in Fig. 9, by decreasing the load, the frequency rises more than to $f_{max} = 51.5$ *Hz*. Therefore, the control system of the PV changes into the non-MPPT mode to keep the frequency at the maximum value. Consequently, the current of PV is decreased from the MPPT value of 3.7 *A* to 2.4 *A*.

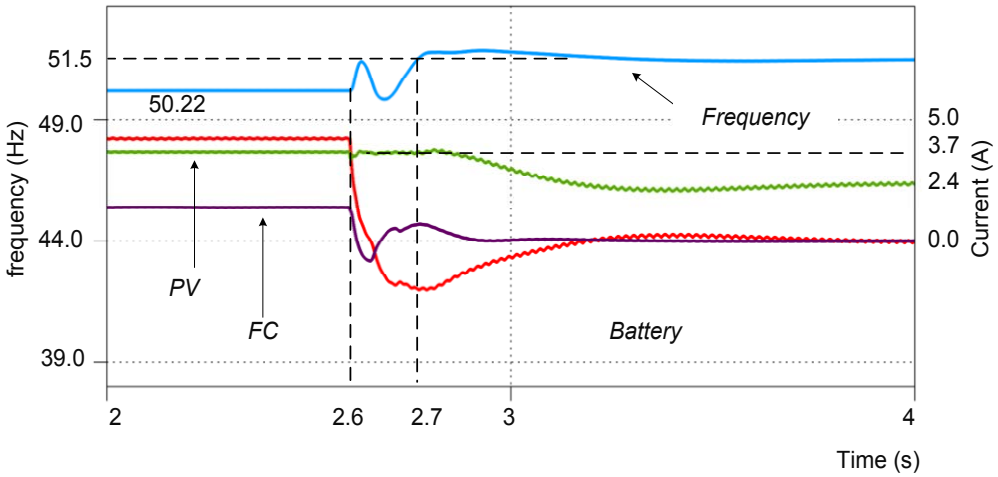

Fig. 9. Simulation results of Case III, one of the loads is disconnected at t = 2.6 *sec*. The output current of PV decreases to settle the frequency at 51.5 *Hz*.

IV. Conclusion

This paper has presented a novel control approach for smart power management in LVDC-MGs. Virtual frequency generated by the battery converter as a master unit, is employed to proportionally control the output current of the other units as well as the exchange of power between the MG and the local grid. Unlike the dc voltage based droop methods, the proposed approach can be employed to smartly control the output power of dispatchable and non-dispatchable units, since the frequency has the same value all over the grid, and hence it cannot be affected by the line impedances. Furthermore, the energy flow among different energy units as well as between the MG and local grid can be properly carried out without using an extra communication network, which may increase the reliability. The viability of the proposed control system is ensured for different loading and sourcing conditions through the simulations.

References

[1] D. Boroyevich, I. Cvetkovic, R. Burgos, and D. Dong, "Intergrid: A Future Electronic Energy Network?," *IEEE J. Emerg. Sel. Top. Power Electron.*, vol. 1, no. 3, pp. 127–138, 2013.

[2] F. Katiraei, R. Iravani, N. Hatziargyriou, and A. Dimeas, "Microgrids Management," *IEEE Power Energy Mag.*, vol. 6, no. 3, pp. 54–65, 2008.

[3] N. Hatziargyriou, H. Asano, R. Iravani, and C. Marnay, "Microgrids," *IEEE Power Energy Mag.*, vol. 5, no. 4, pp. 78–94, 2007.

[4] D. M. Akhil, Abbas A., Georgianne Huff, Aileen B. Currier, Benjamin C. Kaun, "*DOE/EPRI 2013 Electricity Storage Handbook in Collaboration with NRECA,*" no. July. 2013.

[5] B. T. Patterson, "DC, Come Home: DC Microgrids and the Birth of the 'Enernet,'" *IEEE Power Energy Mag.*, vol. 10, no. 6, pp. 60–69, 2012.

[6] Irena, "Battery Storage for Renewables : Market Status and Technology Outlook," 2015.

[7] J. He and Y. W. Li, "Analysis, Design, and Implementation of Virtual Impedance for Power Electronics Interfaced Distributed Generation," *IEEE Trans. Ind. Appl.*, vol. 47, no. 6, pp. 2525–2538, 2011.

[8] P.-H. Huang, P.-C. Liu, W. Xiao, and M. S. El Moursi, "A Novel Droop-Based Average Voltage Sharing Control Strategy for DC Microgrids," *IEEE Trans. Smart Grid*, vol. 6, no. 3, pp. 1096–1106, May 2015.

[9] Y. W. Li and C.-N. Kao, "An Accurate Power Control Strategy for Power-Electronics-Interfaced Distributed Generation Units Operating in a Low-Voltage Multibus Microgrid," *IEEE Trans. Power Electron.*, vol. 24, no. 12, pp. 2977–2988, Dec. 2009.

[10] X. Lu, J. M. Guerrero, K. Sun, and J. C. Vasquez, "An Improved Droop Control Method for DC Microgrids Based on Low Bandwidth Communication With DC Bus Voltage Restoration and Enhanced Current Sharing Accuracy," *IEEE Trans. Power Electron.*, vol. 29, no. 4, pp. 1800–1812, Apr. 2014.

[11] V. Nasirian, A. Davoudi, and F. L. Lewis, "Distributed Adaptive Droop Control for Dc Microgrids," *IEEE*

Trans. Energy Convers., vol. 29, no. 4, pp. 1147–1152, 2014.

[12] H. Nikkhajoei and R. Iravani, "Steady-State Model and Power Flow Analysis of Electronically-Coupled Distributed Resource Units," *IEEE Power Eng. Soc. Gen. Meet. PES*, vol. 22, no. 1, pp. 721–728, 2007.

[13] S. Anand, B. G. Fernandes, and J. M. Guerrero, "Distributed Control to Ensure Proportional Load Sharing and Improve Voltage Regulation in Low-Voltage DC Microgrids," *IEEE Trans. Power Electron.*, vol. 28, no. 4, pp. 1900–1913, 2013.

[14] Q. Shafiee, T. Dragicevic, J. C. Vasquez, and J. M. Guerrero, "Hierarchical Control for Multiple DC-Microgrids Clusters," *IEEE Trans. Energy Convers.*, vol. 29, no. 4, pp. 922–933, 2014.

[15] X. Lu, J. M. Guerrero, K. Sun, J. C. Vasquez, R. Teodorescu, and L. Huang, "Hierarchical Control of Parallel AC-DC Converter Interfaces for Hybrid Microgrids," *IEEE Trans. Smart Grid*, vol. 5, no. 2, pp. 683–692, 2014.

[16] K. Kai Sun, L. Li Zhang, Y. Yan Xing, and J. M. Guerrero, "A Distributed Control Strategy Based on DC Bus Signaling for Modular Photovoltaic Generation Systems With Battery Energy Storage," *IEEE Trans. Power Electron.*, vol. 26, no. 10, pp. 3032–3045, Oct. 2011.

[17] A. Khorsandi, M. Ashourloo, and H. Mokhtari, "A Decentralized Control Method for a Low-Voltage DC Microgrid," *IEEE Trans. Energy Convers.*, vol. 29, no. 4, pp. 793–801, 2014.

[18] P. C. Loh, Y. K. Chia, D. Li, and F. Blaabjerg, "Autonomous Operation of Distributed Storages in Microgrids," *IET Power Electron.*, vol. 7, no. 1, pp. 23–30, 2014.